JACS
JOURNAL OF THE AMERICAN CHEMICAL SOCIETY
Communication
pubs.acs.org/JACS

Photoacoustic Probes for Ratiometric Imaging of Copper(II)

Hao Li,[†] Pamela Zhang,[†] Lukas P. Smaga, Ryan A. Hoffman, and Jefferson Chan*

Roger Adams Laboratory, Department of Chemistry, University of Illinois, 600 South Mathews Avenue, Urbana, Illinois 61801, United States

Supporting Information

ABSTRACT: Photoacoustic tomography has emerged as a promising alternative to MRI and X-ray scans in the clinical setting due to its ability to afford high-resolution images at depths in the cm range. However, its utility has not been established in the basic research arena owing to a lack of analyte-specific photoacoustic probes. To this end, we have developed acoustogenic probes for copper(II)-1 and -2 (**APC-1** and **APC-2**, a water-soluble congener) for the chemoselective visualization of Cu(II), a metal ion which plays a crucial role in chronic neurological disorders such as Alzheimer's disease. To detect Cu(II), we have equipped both APCs with a 2-picolinic ester sensing module that is readily hydrolyzed in the presence of Cu(II) but not by other divalent metal ions. Additionally, we designed **APC-1** and **APC-2** explicitly for ratiometric photoacoustic imaging by using an aza-BODIPY dye scaffold exhibiting two spectrally resolved NIR absorbance bands which correspond to the 2-picolinic ester capped and uncapped phenoxide forms. The normalized ratiometric turn-on responses for **APC-1** and **APC-2** were 89- and 101-fold, respectively.

Photoacoustic tomography (PAT) is a state-of-the-art imaging modality that is based on the detection of ultrasonic waves generated by thermoelastic expansion resulting from the absorption of light and subsequent non-radiative decay.[1,2] In contrast to optical methods such as fluorescence microscopy, in which the typical imaging depth is in the micron regime, PAT can produce high-resolution images in the cm range because sound scatters 3 orders of magnitude less than fluorescence emission in many biological tissues. The anticipated spatial resolution is ~1/200 of the imaging depth, meaning that at 7 cm, the attainable resolution is ~350 μm, whereas at 1 cm, the resolution will be in the 50 μm range.[1] Moreover, because PAT does not involve ionizing radiation, it is potentially less hazardous compared to computed tomography (CT), positron emission tomography (PET), and X-ray scans for medical diagnostic applications. Indeed, PAT has been applied non-invasively to visualize and study various types of cancer,[3] cardiovascular diseases,[4] and abnormalities of microcirculation.[5] To distinguish between physiological and pathological states, many photoacoustic (PA) contrast agents based on small-molecule dyes, metal-based nanoparticles and carbon nanotubes have been developed.[6] Signal enhancement in a specific cell- or tissue-type results from the accumulation of an imaging agent via passive diffusion or receptor-mediated uptake pathways. In contrast, there have been several reports of PA probes that can be activated by a molecular target to elicit a change in the signal intensity.[7−10] Such chemical tools are more versatile than contrast agents because they offer the unique opportunity to interrogate the complex biological role of a given analyte in its native environment with minimal perturbation.[11] To address the lack of available probes, we present the development of two PA probes, acoustogenic probe for copper(II)-1 and -2 (**APC-1** and **APC-2**), for the chemoselective imaging of Cu(II). In this study, we chose to detect Cu(II) because misregulation of this important transition metal ion has been implicated in numerous diseases, including Alzheimer's disease,[12] an area studied by our group.[13] The term "acoustogenic" is used by us to designate any small-molecule-based probe that reacts with a specific molecular target to afford a "turn-on" PA response. APCs are comprised of three components: a Cu(II)-responsive 2-picolinic ester moiety that chelates Cu(II) which activates the ester bond for hydrolysis (Figure 1a, in blue),[14,15] sulfated ethylene glycol functional groups to enhance water solubility (Figure 1a, in red), and a near-infrared absorbing aza-BODIPY dye platform to generate the PA signal (Figure 1a, in black). Of note, maximum absorption in the NIR range (650−900 nm), a large extinction coefficient (>10^4 M^{-1} cm^{-1}) and high photostability are essential properties we considered when developing the APCs.

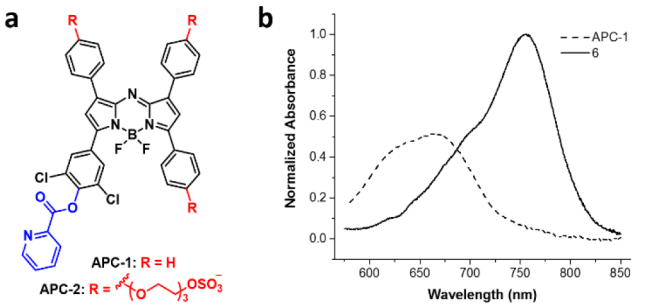

Figure 1. (a) Chemical structures of **APC-1** and **APC-2**. (b) Normalized absorbance spectra of 2 μM **APC-1** (dashed line) and 2 μM **6** (solid line), its hydrolyzed product, in PBS + 0.1% CrEL (pH 7.4).

The aza-BODIPY dye family has been used to construct an assortment of fluorescent probes for reactive sulfur species such as cysteine[16] and hydrogen sulfide,[17] reactive nitrogen species including nitric oxide,[17] nitroxyl,[18] and nitrite,[19] as well as carbohydrates like glucose,[20] but its application for photo-

Received: October 7, 2015

DOI: 10.1021/jacs.5b10504
J. Am. Chem. Soc. XXXX, XXX, XXX−XXX

acoustic imaging has never been reported. In this regard, we selected an aza-BODIPY dye exhibiting dual-wavelength absorbance bands, one below 700 nm and the other above, which correspond to the capped 2-picolinic ester probe (Figure 1b, dotted line) and the uncapped phenoxide product (Figure 1b, solid line), respectively.[21,22] Ratiometric imaging is extremely powerful because it can control for artifacts such as non-uniform dye accumulation and photobleaching. Our strategy involves irradiating a probe, for example **APC-1**, at both the blue-shifted (680 nm) and red-shifted (755 nm) absorbance maxima to generate two corresponding PA signals from which a ratio can be determined (Figure 2). In the absence of Cu(II), the 2-picolinic ester moiety remains intact and thus, the absorbance at 680 nm will be larger than the signal at 755 nm, resulting in a small 755/680 PA ratio (Figure 2). In contrast, when **APC-1** is treated with Cu(II), the hydrolyzed product **6** will exhibit a decrease in the 680 nm band with a concomitant increase in the 755 nm absorbance maximum leading to a large 755/680 PA ratio (Figure 2). Normalization of the two PA ratios will result in the ratiometric turn-on response. In order for this approach to be successfully implemented, the product must be fully deprotonated at physiological pH to ensure that the phenoxide absorbance band is maximized after the ester is cleaved. Thus, we tuned the acidity of the phenol moiety by installing two ortho-chloro substituents. We measured an apparent pK_a value of 4.35, which is consistent with the pK_a for a related aza-BODIPY pH probe recently reported (Figure S1).[21]

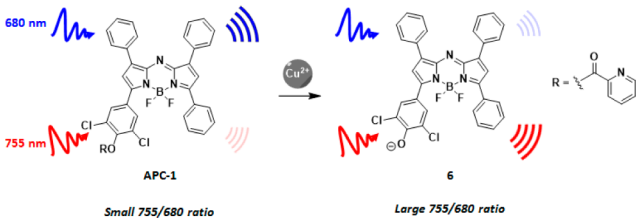

Figure 2. Proposed mechanism for ratiometric PA imaging of Cu(II). **APC-1** (left) is excited at 680 nm (blue) and 755 nm (red) to afford two PA signals. In the presence of Cu(II), the 2-picolinic ester moiety is removed to yield **6** (right), and this results in a weaker PA signal at 680 nm and a stronger PA signal at 755 nm.

First, we synthesized **APC-1** via an EDC-mediated coupling reaction between 2-picolinic acid and the dichlorophenol precursor **6** in 53% yield (Scheme S1). However, because **APC-1** is extremely hydrophobic, organic co-solvents or surfactants were required to achieve sufficient solubility to avoid dye aggregation in aqueous buffers which abolishes the dual-wavelength character requisite for ratiometric imaging. As such, we sought to develop a water-soluble analogue, first by employing previously reported strategies for enhancing the hydrophilicity of aza-BODIPY dyes such as PEGylation[23] and incorporation of amino sulfonic acid moieties.[24] Unfortunately, these approaches were insufficient to adequately solubilize our probe. Instead, we found that three PEG-3 sulfate groups endowed excellent water solubility. As such, **APC-2** was synthesized beginning from the dimerization of 4-nitro-1,3-diphenylbutan-1-one precursors **12** and **15** to afford the tetraarylazadipyrromethene intermediate **16**. To facilitate purification of **16** from homodimers of **12** and **15**, it was necessary to convert the primary alcohols to the corresponding *tert*-butyl dimethylsilyl ether groups using TBS-Cl. The fully TBS-protected tetraarylazadipyrromethene **17** underwent facile boron chelation which was followed by desilylation using TBAF to afford aza-BODIPY **18** in 64% yield. Sulfation of **18** with SO_3−NMe_3 in DMF gave the PEG-3 sulfate intermediate **19**, which was subjected to standard Tsuji−Trost deallylation conditions to give **20** in 74% yield over two steps. Lastly, as before, the 2-picolinic ester was installed using EDC in water to afford **APC-2** in 53% yield (Scheme 1).

Scheme 1. Synthesis of Acoustogenic Probe for Copper(II)-2 (APC-2)

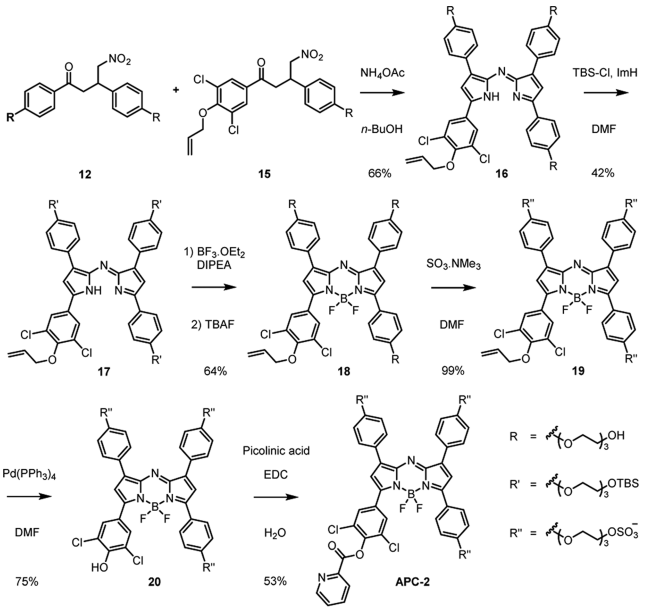

In order to avoid inconsistencies when using different solvents during the spectroscopic characterization and evaluation of each probe, we performed all subsequent assays in PBS with 0.1% CrEL, a potent surfactant used as a vehicle to solubilize poorly water-soluble organic compounds. The absorbance maximum of **APC-2** was centered at 697 nm (ε = 3.6 × 10^4 M^{-1} cm^{-1}), whereas the corresponding maximum of the phenoxide product **20** was 767 nm (3.7 × 10^4 M^{-1} cm^{-1}) (Table S1). We were pleased to discover that both compounds were non-fluorescent in PBS, meaning there would be a greater extent of non-radiative decay correlating to an overall stronger PA signal.[25] However, both APC probes were fluorescent in 2:3 v/v EtOH:PBS, which is consistent with reports from other studies.[21] When **APC-2** was irradiated at its absorbance maximum for 1 h (134 mW/cm^2), we observed only ∼15% loss of fluorescence, demonstrating that **APC-2** is exceptionally photostable (Figure S5). Next, we sought to measure the acoustic emission of **APC-2** as a function of pH when exciting at both the blue- and red-shifted absorbance maxima (Figure 3a,c). When **APC-2** was irradiated at 697 nm, the PA signal was pH insensitive indicating that the 2-picolinic ester trigger is stable across the pH range examined (Figure 3a). Likewise, excitation at 767 nm yielded no observable PA output from pH 3.0 to 8.2, owing to a low extinction coefficient (<2000 M^{-1} cm^{-1}) at this wavelength for the capped probe (Figure 3c). In contrast, when **20** was evaluated at 697 nm, a pH-dependent signal intensity change was noted. In particular, the strength of the PA signal was more prominent in acidic buffers compared to at physiological pH (Figure 3a). Likewise, we also observed a

DOI: 10.1021/jacs.5b10504
J. Am. Chem. Soc. XXXX, XXX, XXX−XXX

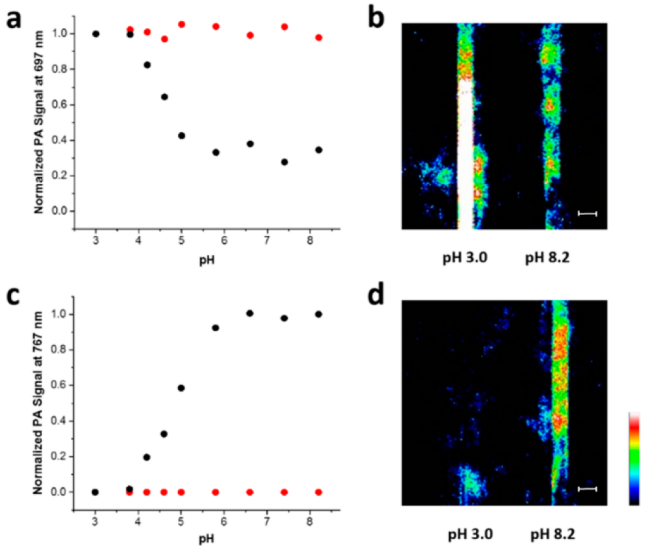

Figure 3. Photoacoustic imaging of **APC-2** and **20** as a function of pH. (a) Normalized pH profile of **APC-2** (red circles) and its hydrolyzed product **20** (black circles), with excitation at 697 nm. (b) Photoacoustic images of 10 μM compound **20** (PBS + 0.1% CrEL, pH 7.4) in FEP tubing overlaid with a 1 cm thick phantom acquired at pH 3.0 and 8.2, with excitation at 697 nm. (c) Normalized pH profile of **APC-2** (red circles) and its hydrolyzed product **20** (black circles), with excitation at 767 nm. (d) Photoacoustic images of 10 μM **20** (PBS + 0.1% CrEL, pH 7.4) in FEP tubing overlaid with a 1 cm thick phantom acquired at pH 3.0 and 8.2, with excitation at 767 nm. Pseudocoloring represents intensity distribution from highest intensity, indicated by white, to the lowest intensity, designated by black. Scale bar represents 2 mm.

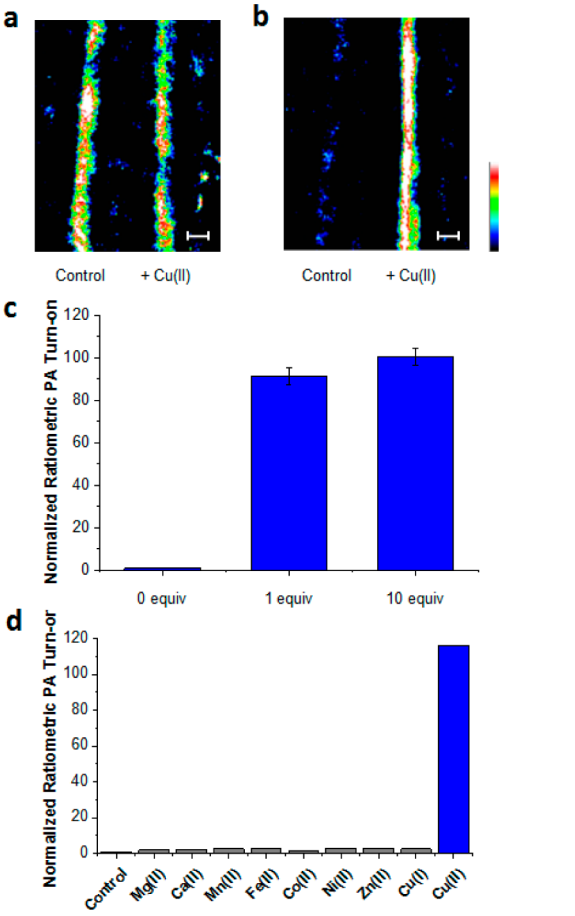

Figure 4. Photoacoustic imaging of **APC-2** treated with Cu(II). Photoacoustic images of 10 μM **APC-2** (PBS + 0.1% CrEL, pH 7.4) in FEP tubing overlaid with a 1 cm thick phantom treated with 0 and 10 equiv of Cu(II), with excitation at (a) 697 and (b) 767 nm. Pseudocoloring represents intensity distribution from highest intensity, indicated by white, to the lowest intensity, designated by black. Scale bar represents 2 mm. (c) Quantification of **APC-2** treated with 0, 1, and 10 equiv of Cu(II) for 90 min. Blue bars represent normalized ratiometric turn-on responses calculated from the PA ratios (PA767/PA697) for control and Cu(II)-treated conditions. n = 2. (d) PA responses of **APC-2** to various metal ions (2 mM for Ca(II) and Mg(II), 50 μM for all other cations).

pH-dependent change in the PA signal with 767 nm excitation. Specifically, at low pHs the PA signal is suppressed, whereas at high pHs the acoustic strength becomes larger (Figure 3c,d). Moreover, we were able to calculate an apparent pK_a value of ~4.5 for the phenol moiety which is consistent with the value obtained from the corresponding absorbance spectrum (Figure 3a,c).

We then turned our attention to evaluating the response of **APC-2** to Cu(II) supplementation using UV−vis spectroscopy. Upon addition of Cu(II), the major visible absorbance band shifted from 697 to 767 nm, indicating facile conversion from **APC-2** to **20** with a rate constant of 2.66 × 10^{-2} min^{-1}. Employing PA imaging, we observed a slight decrease in the PA output at 697 nm when Cu(II) was added (Figure 4a). On the other hand, at 767 nm, a dramatic turn-on response was noted with the Cu(II)-mediated hydrolysis of the 2-picolinic ester moiety (Figure 4b). Normalization of the PA ratios resulted in a ratiometric PA turn-on of 91.3- and 100.5-fold for 1 and 10 equiv of Cu(II), respectively (Figure 4c). Having established excellent responsiveness to Cu(II), we then evaluated the metal ion selectivity by treating solutions of **APC-2** with various biologically relevant metal ions. The PA response of **APC-2** is not affected by the presence of physiologically relevant concentrations of alkaline earth metals such as Mg(II) and Ca(II) or divalent transition metal ions like Mn(II), Fe(II), Co(II), Ni(II), and Zn(II). Moreover, **APC-2** is selective for Cu(II) over Cu(I), showing that this probe has excellent metal and redox specificity (Figure 4d). Of note, we performed competition assays to demonstrate that the presence of the above divalent metal ions do not perturb the reactivity of **APC-2** with Cu(II) (Figure S9). We also determined that **APC-2** responds to Cu(II) complexes of aspartic acid, bilirubin, and clioquinol (Figure S10) and that it is stable in human blood plasma (Figure S11).

To evaluate the PA properties of **APC-2** in the cm range, we developed an agarose-based tissue phantom consisting of milk and water to mimic the light scattering and absorption properties of an authentic tissue sample. Of note, all PA images described in this study were acquired in phantoms cut to a thickness of 1 cm. While the PA signal at this imaging depth remained intense and was clearly visible, the corresponding fluorescence signal was completely abolished when **APC-2** was overlaid with a 1 cm thick phantom (Figure S13). Lastly, we imaged **APC-2** in chicken breast tissue cut to the same dimensions to assess whether the PA signal could be detected in tissue containing lipids, proteins, and blood.[26] Gratifyingly, the PA signal of **APC-2** was comparable to what we observed using the agarose-based phantom (Figure S14).

In closing, we have developed the first small-molecule-based probe exclusively designed for ratiometric photoacoustic

DOI: 10.1021/jacs.5b10504
J. Am. Chem. Soc. XXXX, XXX, XXX−XXX

imaging. **APC-2** displays an absorbance maximum in the NIR window, a large extinction coefficient ($>10^4$ M^{-1} cm^{-1}), and was shown to be extremely photostable. The unique dual-wavelength absorbance profile and low apparent pK_a of the dichlorophenol group produces a large normalized turn-on response of 100.5-fold in the presence of Cu(II). Moreover, we demonstrated that **APC-2** is highly selective for Cu(II) over other biologically relevant metal ions. We also highlight the strength of PA imaging by performing imaging experiments in the cm range using a tissue phantom and authentic tissue. Because this imaging depth is significantly greater than what is possible with optical methods, we anticipate that **APC-2** will open many new opportunities to study the complex biochemistry of Cu(II) in vivo. Indeed, discovering and understanding the influence of an analyte on disease progression is the crucial first step to developing new potential treatment options. On this note, the highly modular aza-BOPIDY platform used in the current study can be easily adapted to sense other biologically important analytes beyond Cu(II) by simply installing alternative reactive triggers at the last step of the synthesis. We anticipate that this initial report will establish a new standard in the PA probe development arena and thus, will be of broad interest to the molecular imaging community. Such probes will be critical for the continued growth of the PA imaging field in both the basic research and clinical settings.

■ ASSOCIATED CONTENT

Supporting Information

The Supporting Information is available free of charge on the ACS Publications website at DOI: 10.1021/jacs.5b10504.

Experimental details, including synthesis of **APC-1** and **APC-2**, and all data for in vitro characterization and imaging experiments (PDF)

■ AUTHOR INFORMATION

Corresponding Author

*jeffchan@illinois.edu

Author Contributions

†H.L. and P.Z. contributed equally to this work.

Notes

The authors declare no competing financial interest.

■ ACKNOWLEDGMENTS

We thank Dr. Michael Thornton (Endra Life Sciences) for helpful scientific discussions and assistance with imaging experiments. We thank Ms. Chelsea Anorma for assisting with the fluorescence imaging experiments. P.Z. acknowledges the United States Air Force for a graduate fellowship. R.A.H. thanks the Researchers Initiative Program for research experience for undergraduates (REU) funding.

■ REFERENCES

(1) Wang, L. H. V.; Hu, S. *Science* **2012**, *335*, 1458.
(2) Xia, J.; Yao, J. J.; Wang, L. V. *Prog. Electromagn. Res.* **2014**, *147*, 1.
(3) Mallidi, S.; Luke, G. P.; Emelianov, S. *Trends Biotechnol.* **2011**, *29*, 213.
(4) Zemp, R. J.; Song, L.; Bitton, R.; Shung, K. K.; Wang, L. V. *Opt. Express* **2008**, *16*, 18551.
(5) Luke, G. P.; Yeager, D.; Emelianov, S. Y. *Ann. Biomed. Eng.* **2012**, *40*, 422.
(6) Wu, D.; Huang, L.; Jiang, M. S.; Jiang, H. B. *Int. J. Mol. Sci.* **2014**, *15*, 23616.
(7) Dragulescu-Andrasi, A.; Kothapalli, S. R.; Tikhomirov, G. A.; Rao, J. H.; Gambhir, S. S. *J. Am. Chem. Soc.* **2013**, *135*, 11015.
(8) Pu, K. Y.; Shuhendler, A. J.; Jokerst, J. V.; Mei, J. G.; Gambhir, S. S.; Bao, Z. N.; Rao, J. H. *Nat. Nanotechnol.* **2014**, *9*, 233.
(9) Cash, K. J.; Li, C. Y.; Xia, J.; Wang, L. H. V.; Clark, H. A. *ACS Nano* **2015**, *9*, 1692.
(10) Levi, J.; Kothapalli, S. R.; Ma, T. J.; Hartman, K.; Khuri-Yakub, B. T.; Gambhir, S. S. *J. Am. Chem. Soc.* **2010**, *132*, 11264.
(11) Chan, J.; Dodani, S. C.; Chang, C. J. *Nat. Chem.* **2012**, *4*, 973.
(12) Manto, M. *Toxics* **2014**, *2*, 327.
(13) Roth, A.; Li, H.; Anorma, C.; Chan, J. *J. Am. Chem. Soc.* **2015**, *137*, 10890.
(14) Fife, T. H.; Przystas, T. J. *J. Am. Chem. Soc.* **1985**, *107*, 1041.
(15) Kierat, R. M.; Kramer, R. *Bioorg. Med. Chem. Lett.* **2005**, *15*, 4824.
(16) Jiang, X. D.; Zhang, J.; Shao, X. M.; Zhao, W. L. *Org. Biomol. Chem.* **2012**, *10*, 1966.
(17) Adarsh, N.; Krishnan, M. S.; Ramaiah, D. *Anal. Chem.* **2014**, *86*, 9335.
(18) Liu, P.; Jing, X. T.; Yu, F. B.; Lv, C. J.; Chen, L. X. *Analyst* **2015**, *140*, 4576.
(19) Adarsh, N.; Shanmugasundaram, M.; Ramaiah, D. *Anal. Chem.* **2013**, *85*, 10008.
(20) Liu, Y. L.; Zhu, J. W.; Xu, Y. M.; Qin, Y.; Jiang, D. C. *ACS Appl. Mater. Interfaces* **2015**, *7*, 11141.
(21) Strobl, M.; Rappitsch, T.; Borisov, S. M.; Mayr, T.; Klimant, I. *Analyst* **2015**, *140*, 7150.
(22) Jokic, T.; Borisov, S. M.; Saf, R.; Nielsen, D. A.; Kuhl, M.; Klimant, I. *Anal. Chem.* **2012**, *84*, 6723.
(23) Collado, D.; Vida, Y.; Najera, F.; Perez-Inestrosa, E. *RSC Adv.* **2014**, *4*, 2306.
(24) Kamkaew, A.; Burgess, K. *Chem. Commun.* **2015**, *51*, 10664.
(25) Kim, C.; Favazza, C.; Wang, L. H. V. *Chem. Rev.* **2010**, *110*, 2756.
(26) Ku, G.; Wang, L. H. V. *Opt. Lett.* **2005**, *30*, 507.

DOI: 10.1021/jacs.5b10504
J. Am. Chem. Soc. XXXX, XXX, XXX−XXX